Supplementary information

Designed fabricated of Networked Mn(II)-Magnetic-Chitosan Bio-composite towards Highly Efficient and Rapid Degradation of Dye without Heating or Light and Aerobic Selective Oxidation of Ethylbenzene

Behzad Bornas[a], Alireza Faraji*[,a,b] Fatemeh Ashouri[c]

[a]*Department of Organic Chemistry, Faculty of Pharmaceutical Chemistry, Tehran Medical Sciences, Islamic Azad University, Tehran, Iran.*
[c]*Department of Applied Chemistry, Faculty of Pharmaceutical Chemistry, Tehran Medical Sciences, Islamic Azad University, Tehran, Iran.*

Corresponding author. Tel.: +98 21 22640051; fax: +98 21 22600099.
E-mail address: alireza_ch57@yahoo.com, a.faraji@iaups.ac.ir.

Text 1S. Preparation of MIOSC NPs

In the first stage, 2.0 g $FeCl_2 \cdot 4H_2O$ and 5.2 g $FeCl_3 \cdot 6H_2O$ ($n\mathrm{Fe}^{3+}/n\mathrm{Fe}^{2+} = 2$) were dissolved in a mixture of chloric acid (0.1 M) and deionized water (DI H_2O, 25 mL). Meanwhile, the obtained solution was stirred under the N_2 atmosphere at 80 ºC, and then 25 mL of NaOH (1.5 M) drop by drop were added to the solution. After a short while, MIO NPs appeared as dark brown sediment and were separated by a super magnet. The MIO NPs were washed by H_2O/EtOH (1:1) three times and dried at 60 ºC. The modified Stöber sol-gel method was applied to prepare MIO NPs coated by monodispersed silica. 1.0 g of the dark brown sediment was dispersed to the mixture of 4.0 mL ammonia (25%), 20 mL EtOH. The mixture was sonicated in the ultrasonic for 15 min. Then, 0.6 mL TEOS was injected into the solution.

Text 2S. Identification and isolation of AP

The presence of AP (acethophenone), PEA (phenyl ethyl alcohol), Bz (benzaldehyde) & BZ (benzoic acid) were identified by GC & GC-MS. It must be noted that di(1-phenylethyl) ether, 2,3-diphenyl butane & over-oxidation of AP (methyl benzoate) were not detected. Additionally, the effect of various pivotal parameters has been assessed to determine optimal reaction conditions. The conversion (X) was calculated on the basis of changes in the relative areas (%) of the EB and products (AP, PEA, BZ & BZ) peaks according to equation 2:

For isolation of AP, the reaction mixture was concentrated and dispersed in EtOH (20 mL). Then 66.0 mg of Zn was dispersed in EtOH by ultrasonication and it was added drop-wise to the ethanol solution of the previous step, and then it was vigorously stirred at room temperature for 0.5 hr. Immediately after filtration, the solution was distilled at 80 °C for removing the EtOH. Next, it was reacted with 30 mL of the saturated solution of sodium bicarbonate (7.5 g $NaHCO_3$ in 50 mL H_2O) for the dissolution of BZ in the aqueous phase. After separation of the aqueous phase, the organic phase was washed with deionized H_2O (4 ×15), subsequently extracted with EtO_2. The organic phase is dried over anhydrous $MgSO_4$ and the solvent was evaporated at room temperature. The achieved light yellow oil contains AP which was identified by FT-IR and LC-MS techniques.

Text 3S. Apparatuses

ICP-OES (inductively coupled plasma-optical emission spectroscopy, Perkin-Elmer ICP/6500), AAS (atomic absorption spectroscopy, Analytik Jena-nov AA300), EDX (Energy-Dispersive X-ray). Furthermore, the constructed polymer-coated magnetic catalysts were identified by various analyze (i.e. FT-IR (Fourier-Transform Infrared, Shimadzu Varian 4300Fourier Transform Infrared spectrometer, KBr pellets), UV–vis (Ultraviolet-visible, SHIMADZU-UV-1800, UV-visible espectrophotometr equipped with a diffuse reflectance), TGA (Thermogravimetric Analysis, Perkin-Elmer TG-DTA 6300, heating rate of 15 °C/min), XRD (X-Ray Diffraction, Bruker D8 Advance diffractometer, CuKa radiation, 40 Kv, 20 miliamper), VSM (Vibrating-Sample Magnetometer, BHV-55 VSM), and XPS (X-Ray Photoelectron Spectroscopy, PerkinElmer PHI 5000CESCA system, B.P= 9-10 Torr). The DLS (Dynamic Light Scattering, (DLS, Zetasizer Nano-ZS-90 (ZEN 3600,Malvern Instrument));   SEM (Transmission Electron Microscopy, Tecnai F30TEM operating at 300 Kv), TEM (Transmission Electron Microscopy, Philips 501 microscope ,80 kV voltage) provided direct visualization of the morphology and size of the MIOSC-N-et-NH$_2$@CS-Mn(II).

Text 4S. Leaching and heterogeneity test

A Sheldon test was applied to assess the heterogeneity and/or Leaching test of the MIOSC-N-*et*-NH$_2$@CS-Mn. The reactions of discoloration of methyl orange and aerobic oxidation of ethylbenzene were divided into two-halves after 3.0 min and 2.0 h from the beginning of the catalytic process, respectively. In one-half, the MIOSC-N-*et*-NH$_2$@CS-Mn was separated by bare magnet from the reaction medium and the reaction was proceeded (5.0 min for degradation process & 1.0 h for aerobic oxidation of ethylbenzene), which results confirmed that no progress has been done in catalyst-free condition. These data shown that no leaching of Mn carried out into the filtrate solution, thus, these observations justified the true-heterogeneity of MIOSC-N-*et*-NH$_2$@CS-Mn. Additionally, to study of reusability of MIOSC-N-*et*-NH$_2$@CS-Mn, the bio-composite was separated magnetically, washed thoroughly, dried and reused in consecutive runs.

Text 5S. Response surface method (RSM)

The second-order RE (%) to predict the catalytic decolorization of MO in terms of coded and actual factors are as below:

Removal efficiency (%) = +100.00 +22.85 A +27.09 B +7.98 C +34.26 F +9.13AB +14.38 AF +20.25 BF-20.34 A^2 -29.01 B^2 -10.14 C^2 -9.77 D^2 -38.29 F^2

where RE (%) is the response factor in peak area and *A*, *B*, *C, D, E* and *F* are the independent factors of PMS dosage, MIOSC-N-*et*-NH$_2$@CS-Mn loading, time, temprature, pH, and MO dosage. Base of analysis of variance (ANOVA) for response surface quadratic model. The R^2 (coefficient of determination) and Adjusted-R^2 was 0.9641 confirming the model were suitable to represent the factors for MIOSC-N-*et*-NH$_2$@CS-Mn.

T

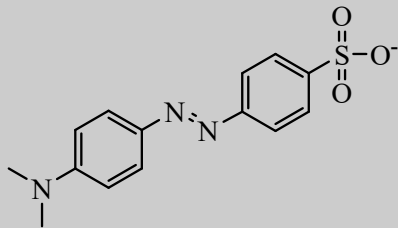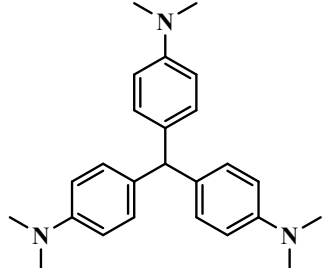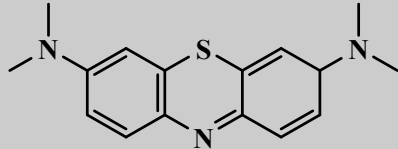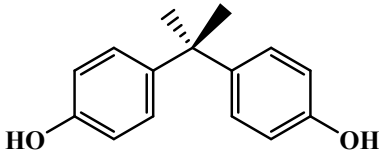**Table 1S.** Chemical structures and capabilities of the selected pollutants.

Sample	λ_{max} (nm)	Mw (g/mol)	Name (IUPAC)	Molecular structure
Methylene orange (MO)	466	327.33	Sodium 4-{[4-(dimethylamino)phenyl]diazenyl}benzene-1-sulfonate	
Methyl violet (MV)	585	357.5	4-[[4-(dimethylamino)phenyl]-(4-methyliminocyclohexa-2,5-dien-1-ylidene)methyl]-N,N-dimethylaniline	
Methylene blue (MB)	664	319.85	[7-(Dimethyl- amino)phenothiazin-3-ylidene]-dimethyla- zanium chloride	
Bisphenol A (BPA)	265	228.29	4-[2-(4-hydroxyphenyl)propan-2-yl]phenol	

Table .2S. Comparison of energy activation and thermodynamic prpperties of MIOSC-N-*et*-NH$_2$@CS-Mn in MO degradation with other heterogeneous system.

Entry	Catalytic System	E_a (kJ/mol)	ΔH (kJ/mol)	ΔS (kJ/mol K)	[Ref]
1	S-1 CuO/H$_2$O$_2$	59.84	57.20	-0.0962	[1]
2	CuNPs/PMS	13.19	11.39	-0.25848	[2]
3	CuNPs/PDS	21.64	19.12	-0.24268	[2]
4	HCF(III)[a]	79.09	76.41	-0.00498	[3]
5	MIL-10-DCD-1000/PMS[b]	18.70	NR[c]	NR	[4]
6	FeCo-MCM-41/PMS	17.20	NR	NR	[5]
7	MIOSC-N-et-NH$_2$@CS-Mn/PMS	35.62	38.61	−0.12171	**This work**

[a]Hexacyanoferrate (III).

[b]Dicyandiamide immobilized on the surface of carbon cloth.

[c]Not reported.

Table 3S. Comparison of energy activation of MIOSC-N-*et*-NH$_2$@CS-Mn in aerobic oxidation of EB with other heterogeneous system.

Entry	Catalytic System	E_a (kJ/mol)[a]	[Ref]
1	3/3-IRA-900/TBHP	33.6 ± 7.5	[6]
2	CuMgAl-LDH/NHPI	35.2	[7]
3	Co-Cu/SAPS-15/TBHP	37.098	[8]
4	Co-N/C-700/TBHP	22.2 ± 2.1	[9]
5	MIOSC-N-*et*-NH$_2$@CS-Mn/NDHPI	22.59	This study

[a]Energy activation

Table. 4S. The aerobic oxidation of EB Catalyzed by MIOSC-N-*et*-NH$_2$@CS-Mn nanocomposite.

No.	Solvent[a]	X [%]	S_{AP} [%]
1	MeOH	21.3	32.9
2	EtOH	16.0	26.8
3	HAc	90.3	93.8
4	BZ	21.4	31.4
5	DCM	41.3	36.0
6	TCM	47.2	45.7
7	1,2-DCM	29.6	39.1
8	CY	54.4	36.8
9	ACN	63.4	48.2
10	TOL	44.7	12.0
11	Bz	36.6	53.9
12	HAc-H$_2$O (1:2)	32.9	34.2
13	HAc-H$_2$O (1:1)	47.2	37.9
14	HAc-H$_2$O (2:1)	94.0	95.0
15	HAc-H$_2$O (1.5:1)	93.7	95.1

[a] Reaction conditions: [EB]= 2 mmol; [MIOSC-N-*et*-NH$_2$@CS-Mn] = 60 mg, V$_{solvent}$= 5.0 mL, [NDHPI]=400 mg; *t*=5 h, T = 80 °C; under O$_2$ bubbling.

Table 5S. Comparison of catalytic activity of MIOSC-N-*et*-NH$_2$@CS-Mn whit various catalytic systems in degradation of pollutants reported in literature.

S.	Catalytic System	t (min)	Oxidant [c]	Efficiency (%)	pH	Ref
MB	5% Mn@Carbon Composite [0.5g/L]	120	PMS [1.0 g/L]	88.16	NR	[10]
	Cu@Co-MOFs-3[0.2 g/L] [1]	30	PMS [2.0 mM]	100	11.0	[11]
	Mn$_3$O$_4$[0.12 g/L]	60	PMS [0.94 g/L]	88.64	4.00	[12]
	elbaite[1g/L]	15	PMS [0.5 g/L]	100	2.90	[13]
	5% MnO$_2$@SBC[0.3g/L] [2]	180	PMS [0.5 mM]	100	7.50	[14]
	CuFe$_2$O$_4$@GO[0.2 g/L] [3]	30	PMS [0.8 mM]	93.3	7.00	[15]
	CNTs-CoFe$_2$O$_4$@PPy[1.0g/L] [4]	30	PMS [4.0 mM]	100	7.00	[16]
	MnCo$_2$O$_{4.5}$[20mg/L]	25	PMS [0.5g/L]	100	NR	[17]
	FeMnO$_3$[0.2g/L]	60	PMS [2.0 g/L]	98	6.70	[18]
	Fe$_3$O$_4$@MnO$_2$[300mg/L]	30	PMS [20 mM]	100	7.94	[19]
	This work	14	PMS[2.0 mM]	97.6	7.00	-
MO	MnCo$_2$O$_{4.5}$[20mg/L]	6	PMS [0.5 g/L]	96.3	NR	[17]
	OMS-2/CNFs[0.2g/L] [5]	30	PMS [0.2 g/L]	~ 90	7.00	[20]
	Co-Mn LDH[0.025 g/L] [6]	4	PMS [0.1 g/L]	100	6.87	[21]
	CC-MIL-10-DCD-1000[0.1 g/L] [7]	30	PMS [0.3 mM]	<95	7.00	[13]
	ACP-800 [0.5 g/L] [8]	80	PMS [3.0 mM]	100	3.5	[22]
	CuAl–LDH[20mg]	10	H$_2$O$_2$ [0.5mL]	99.10	~7.0	[23]
	FeCo-MCM-41 [0.2g/L] [9]	60	PMS [0.075 mM]	<90	5.60	[14]
	Fe$_2$MnO$_4$/AC-H[2.5g/L] [10]	60	H$_2$O$_2$ [1.8×10^{-2} mol/L]	100	3.00	[24]
	This work	8	PMS[2.0 mM]	98.8	7.00	-
BPA	Mn$_{0.8}$Fe$_{2.2}$O$_4$ MNCs[0.5 g/L] [11]	20	PMS [0.4 mM]	100	10.2	[25]
	p-Mn/Fe$_3$O$_4$[0.2 g/L]	30	PMS [2.0 mmol/L]	100	11.0	[26]
	Mn-Fe LDO[0.4 g/L] [12]	50	PMS [1.5 mM]	100	7.00	[27]
	Fe/Mn@NBC800[0.2g/L] [13]	20	PMS [3.0 mM]	100	6.85	[28]
	p-Mn$_1$Fe$_1$ NCs[0.3g/L] [14]	30	PMS [2.0 mM]	100	7.00	[29]
	MnFe$_2$O$_4$@BC[0.2g/L]	30	PMS [0.2 g/L]	100	7.00	[30]
	Mn-Fe$_2$O$_3$[0.5g/L]	30	PMS [0.1 g/L]	99.0	8.00	[31]
	13%-Mn-FeBC[0.5 g/L] [15]	120	PMS [4.0 mM]	100	12.0	[32]
	FeMn@CN-800[50mg/L] [16]	60	PMS [0.20g/L]	95.4	5.60	[33]
	This work	10	PMS[2.0 mM]	98.4	7.00	-
MV	Fe$_3$O$_4$@MnO$_2$[300mg/L]	30	PMS [20.0 mM]	100	7.94	[19]
	MnFe$_2$O$_4$-rGO [0.05 g/L]	30	PMS [0.5 mg/L]	-	97.0	[34]

Fe^0@GG-*cl*-SY NCH [30 mg] [17]	120	H$_2$O$_2$ [5.0 mL/L]	Natural	81.0	[35]
CeVO$_4$[1.0 g/L]	40	PMS [2.0 g/L]	-	100	[36]
Ni$_2$P[150 mg/L][18]	12	PMS [150 mg/L]		35.67	[37]
UCN@COF[0.10 g/L] [19]	90	PMS[0.65 mM]	5.88	96.2	[38]
This work	14	PMS[2.0 mM]	95.7	7.00	-

[1] Cu particle-doped cobalt-based metal–organic framework (Cu@Co-MOF).

[2] Sludge biochar by MnO$_2$.

[3] Copper ferrite-graphite oxide hybrid.

[4] Polypyrrole/CNTs-CoFe2O4 magnetic nanohybrid.

[5] Manganese (III) species in manganese oxide octahedral molecular sieve by interaction with carbon nanofibers.

[6] Co-Mn layered double hydroxide.

[7] Fe/N-codoped carbocatalysts loaded on carbon cloth.

[8] Activated carbon using pistachio (ACP).

[9] Fe-Co bimetal-doped MCM-41.

[10] Magnetic Fe2MO4 (M: Fe, Mn) activated carbons.

[11] Mn/Fe MOF-templated.

[12] Mn–Fe layered double oxides.

[13] Nitrogen-doped biochar encapsulated Fe/Mn nanoparticles.

[14] Porous Mn-Fe nanocubes.

[15] Coupling of KMnO$_4$-assisted sludge dewatering and pyrolysis to prepare Mn, Fe-codoped biochar.

[16] Fe/Mn-loaded nitrogen-doped porous carbonaceous materials.

[17] Zero valent iron@ guar gum crosslinked soya lecithin nanocomposite hydrogel.

[18] Nickel Phosphide with Dual Active Sites

No	Catalytic system	X [%]	S [%]	[Ref]
1	Ce-BTC[1] [0.07 mg],160 ºC, 20h, solvent-free, O_2	84.99	95.63	[39]
2	3/3-IRA-900[0.1 g],100 ºC,12h,solvent-free,TBHP	83.5	93.3	[6]
3	LDH-[NAPABA-Co[II]][2] [100 mg],120 ºC,7h,solvent-free,TBHP	67.4	99.57	[40]
4	Ti–Zr–Co [20 mg],170,4.5h,CH_3CN,O_2	61.9	69.2	[41]
5	Al_2O_3@CoCuAl-MMO6 [0.1g],120 ºC,12h,solvent-free,TBHP	92.8	89.4	[42]
6	Co-N-C0.15 /CNTs[3] [30 mg],120 ºC,5h,solvent-free,O_2	19.9	72.9	[43]
7	Co[II]0.1mol%/NHPI [1.0 mol%],80 ºC,6h, solvent free,O_2	35.0	83.0	[44]
8	CoPcTs-Zn2Al-LDH[4][30 mg]/NHPI 0.4mmol,120 ºC,12h,Benzonitrile,O_2	90.0	99.0	[45]
9	Mn TCPP/pd-CTS[5],155 ºC,2.5h,solvent-free,O_2[0.8 MPa]	20.74	53.91	[46]
10	CoSACs[6] [2.0 mg],120 ºC,24h,solvent-free,air atmosphere	46.0	97.0	[47]
11	Mg_2Fe-LDH [0.1 g]/NHPI [0.1 mol],80 ºC,10h,Trifluorotoluene,O_2	7.40	86.2	[48]
12	Co_2Al-LDH [0.1 g]/NHPI [0.1 mol],80 ºC,10h,Trifluorotoluene,O_2	34.6	85.2	[49]
13	CoTPPs/Mesp-CTS[7] [0.72×10^{-6} mol],140 ºC,4h,solvent free,O_2	42.8	65.4	[50]
14	FeTCPP/Mesp-CTS[8],145 ºC,4h,solvent free,O_2	24.4	74.3	[50]
15	SiO_2/Al_2O_3-APTMS_BPK-Mn[II][9]/NHPI[15%],100,8h,acetic acid,O_2	53.0	74.0	[51]
16	Mn[Ac]$_2$.4H_2O [0.2 g],130 ºC,8h,solvent free,O_2 [1.0] Mpa	45.5	78.8	[52]
17	Mn-ZSM-5-50 [10] [100 mg],80 ºC,6h,CH_3CN,TBHP	43.6	68.8	[53]
18	NS-CSs [11][0.01g],80 ºC,10h,H_2O,TBHP	93.9	94.2	[54]
19	LDH-Si[ph]-Mn-3[6][12] [0.2] g/TBHP 30 mg,130 ºC,5h,solvent-free,O_2	18.0	95.8	[55]
20	Mn[II]-Met@MMNPs[13] [100 mg]/NHPI15%,100 ºC,8h,HOAc,O_2	85.0	98.0	[56]
21	PdPc@CA[14] [0.036 mmol],reflux,24,solvent-free,O_2	73.0	100	[57]
22	Mn/N-C/Al_2O_3 [50 mg],120 ºC,6h,solvent-free,O_2	27.8	>99	[58]
23	MIOSC-N-*et*-NH_2@CS-Mn [40 mg],80 ºC,5.0 h, acetic acid/water,O_2	93.7	95.1	**This work**

Table 6S. Comparison of catalytic activity of MIOSC-N-*et*-NH_2@CS-Mn whit various catalytic systems in EB oxidataion reported in literature.

[1] BTC:1,3,5-benzenetri carboxylic acid

[2] LDH-hosted Co[(II)] Schiff base of 2-hydroxy-1- naphthaldehyde and 4-amino benzoic acid

[3] Co-N-C immobilized carbon nanotubes (CNTs)

[4] Metallophthalocyanine Intercalated Layered Double Hydroxide

[5] manganese porphyrin is promoted by the axial nitrogen coordination in powdered chitosan

[6] cobalt single atom site

[7] Mesoporous Chitosan-Grafted Cobalt Tetrakis(p-Sulfophenyl) Porphyrin

[8] Mesoporous chitosan-immobilized iron tetrakis(4- carboxyphenyl)porphyrin

[9] Mn supported on SiO_2-Al_2O_3

[10] tetrahedral coordination manganese-incorporated ZSM-5 zeolite (Mn-ZSM-5).

[11] Nitrogen and Sulfur Co-Doped Carbon Nanospheres.

[12] Mn-containing silylated MgAl layered double hydroxides.

[13] Organosuperbase dendron manganese complex grafted on magnetic nanoparticles.

[14] cross-linked chitosan aerogel modified with Pd(II)/phthalocyanine.

Table 7S. Commercial price and amount of chemical reagents used.

Material	CAS. Number	Volume/Weight	Price ($/g)
$FeCl_2 \cdot 4H_2O$	13478-10-9	0.3 g	0.030
$FeCl_3 \cdot 6H_2O$	10025-77-1	0.7 g	0.110
HCl	Dr Mojallali,Co.	3.0 mL	0.003
NaOH	Arvandparak, Co.	6.0 g	0.053
$NH_4 OH$	Dr Mojallali,Co.	4.0 mL	0.013
EtOH	Simin Tak, Co.	80 mL	0.260
TEOS	78-10-4	0.6 mL	0.050
APTS	13822-56-5	0.1 mL	0.050
Chitosan	9012-76-4	0.10 g	0.017
AcOH	64-19-7	0.4 mL	0.030
Glutaraldehyde (50 %)	111-30-8	2.0 mL	0.160
$Mn(OAc)_2$	6156-78-1	0.50 g	0.020
		Total price ($)	0.794

Table.8S. Screening data for the cost of the various systems for degradation of $1m^3$ wastewater.

No.	Pollutant/m^3	Catalytic system	Cost ($ /m^3)	[Ref]
1	Tetracycline	PS+γ-Fe$_2$O$_3$-CeO$_2$	0.106	[59]
2	Ketoprofen	PS+Fe^{2+}	0.517	[60]
3	Ketoprofen	PS+Thermal	44.41	[60]
4	Ketoprofen	PS+UV	0.176	[60]
5	Methyl orange	PMS+MIOSC-N-et-NH$_2$@CS-Mn	26.46	*This work*
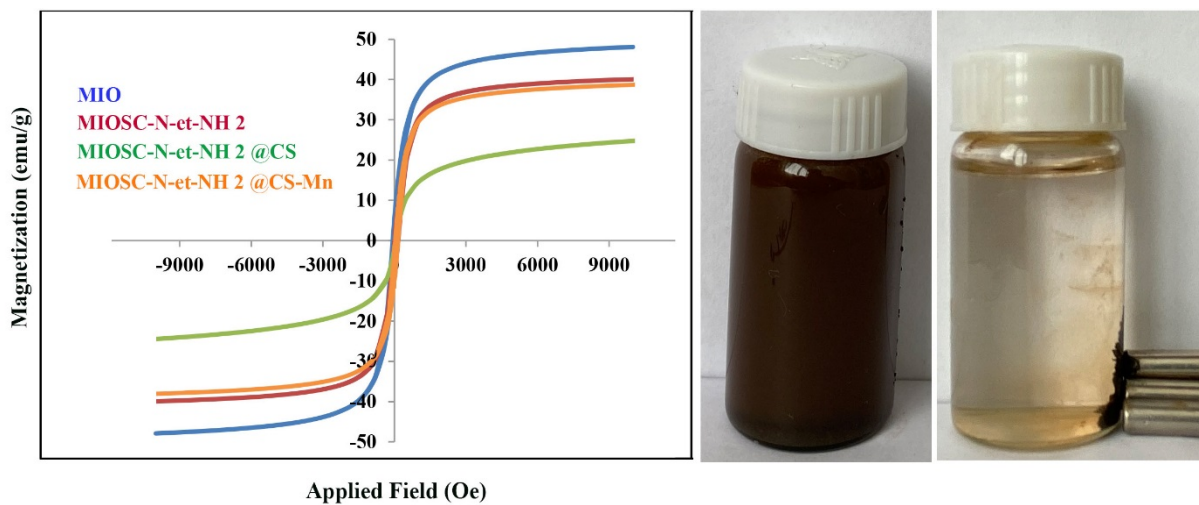
Fig 1S. Magnetic properties of MIONPs, MIOSC-N-*et*-NH$_2$, MIOSC-N-*et*-NH$_2$@CS and MIOSC-N-*et*-NH$_2$@CS-Mn.
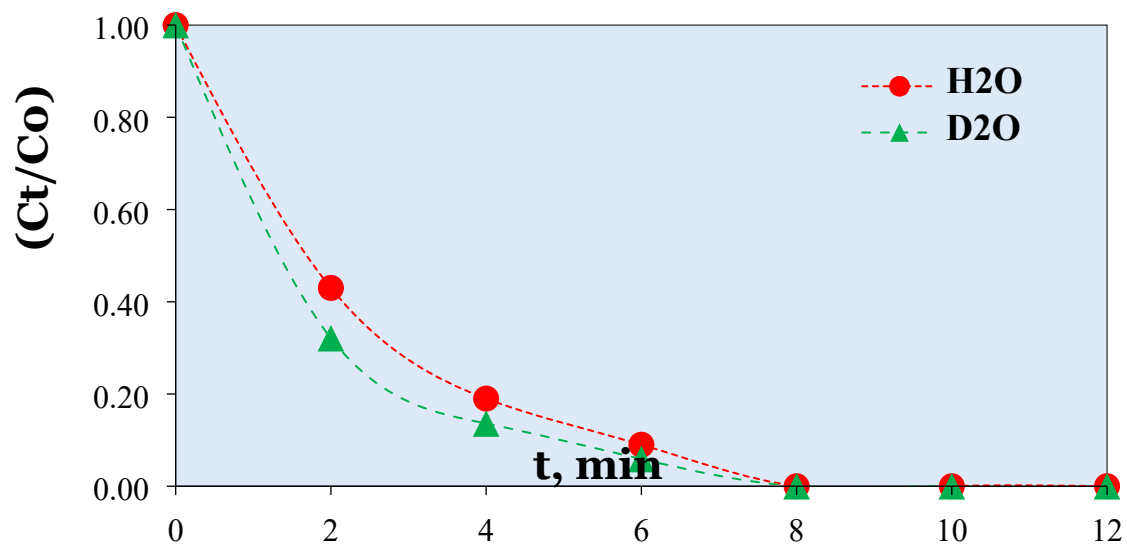
Fig .2S . Re

moval efficiency of degradation of MO by MIOSC-N-*et*-NH$_2$@CS-Mn in H$_2$O and D$_2$O.
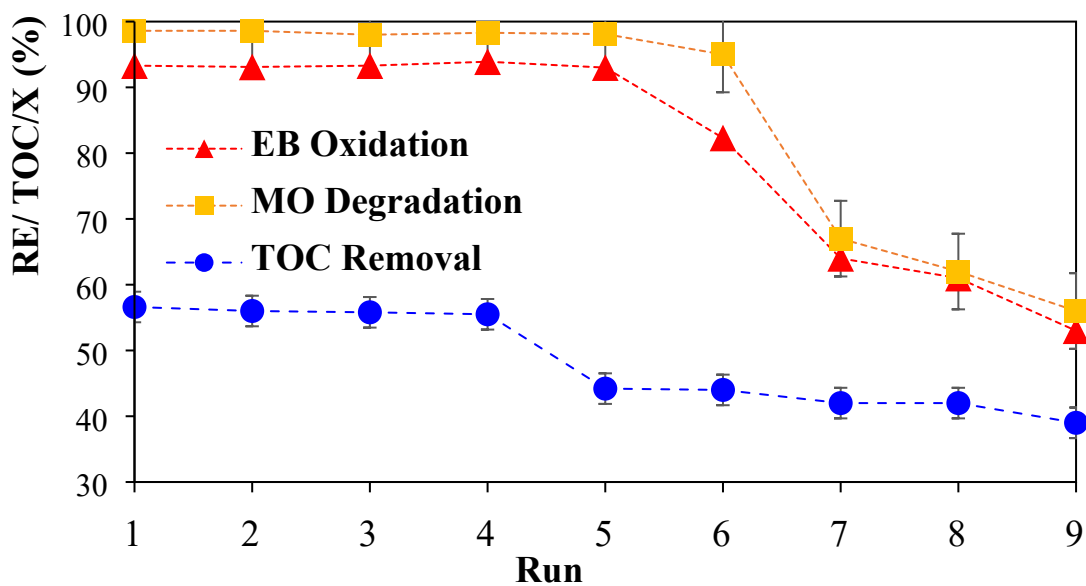
Fig. 3S. Efficiency of MIOSC-N-*et*-NH$_2$@CS-Mn in MO degradation, EB oxidation and TOC removal.
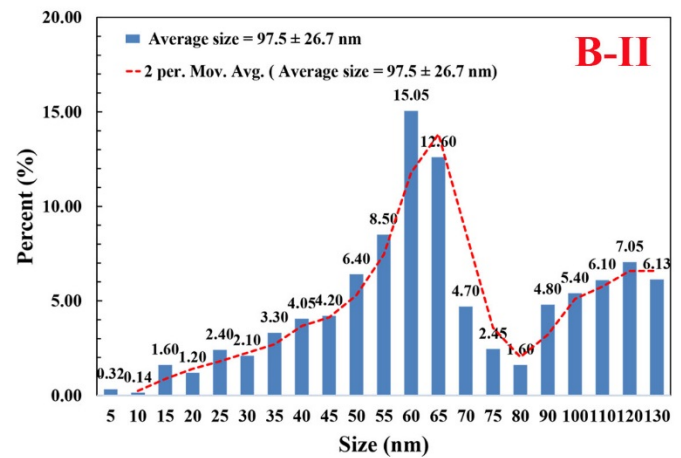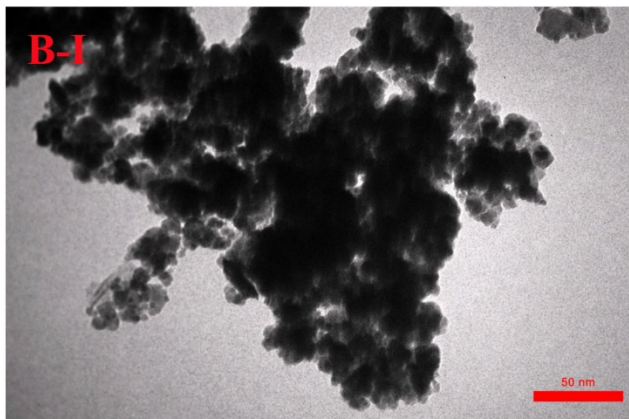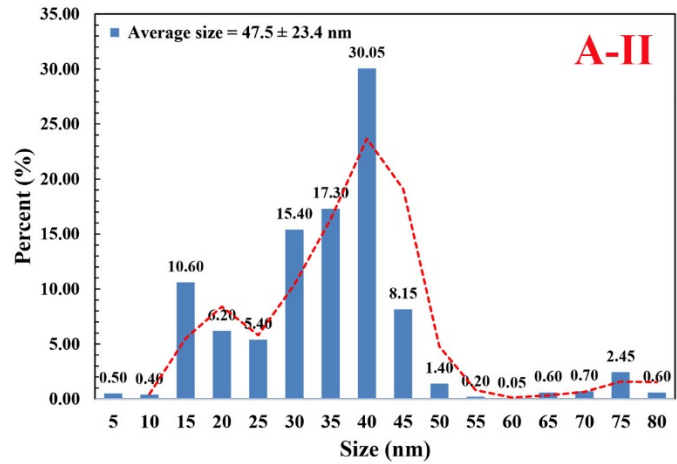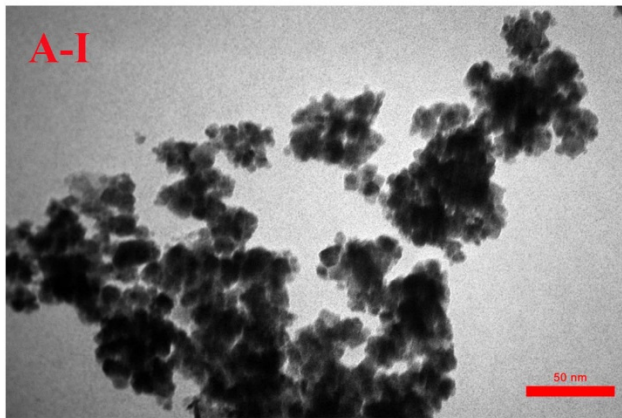
Fig 4S. TEM image and DLS analysis of MIOSC-N-*et*-NH$_2$@CS-Mn after (**A**) 6 run, and (**B**) 8 run.

References

[1] Deka P, Hazarika A, Deka RC, Bharali P. Influence of CuO morphology on the enhanced catalytic degradation of methylene blue and methyl orange. RSC advances. 2016;6(97):95292-305.

[2] Nagar N, Devra V. Activation of peroxodisulfate and peroxomonosulfate by green synthesized copper nanoparticles for Methyl Orange degradation: a kinetic study. Journal of environmental chemical engineering. 2017 Dec 1;5(6):5793-800.

[3] Goel A, Bhatt R, Rani N. Removal of methyl orange, an azo dye, using oxidative degradation by hexacyanoferrate (III) ions. InDiscovery Science 2012 (Vol. 2, No. 4, pp. 32-36).

[4] Yang L, Chen W, Sheng C, Wu H, Mao N, Zhang H. Fe/N-codoped carbocatalysts loaded on carbon cloth (CC) for activating peroxymonosulfate (PMS) to degrade methyl orange dyes. Applied Surface Science. 2021 May 30;549:149300.

[5] Sun X, Xu D, Dai P, Liu X, Tan F, Guo Q. Efficient degradation of methyl orange in water via both radical and non-radical pathways using Fe-Co bimetal-doped MCM-41 as peroxymonosulfate activator. Chemical Engineering Journal. 2020 Dec 15;402:125881.

[6] Wang Z, Jiang Y, Huo H, Hu Y, Xu X, Wang P, Yang Y, Lin K. Synthesis of three-dimensional nitrogen doped meso/macroporous carbon beads for heterogeneous catalytic solvent-free oxidation of ethylbenzene. Carbon. 2020 Mar 1; 158:226-37.

[7] Dai X, Li X, Tang S, Peng X, Zheng X, Jiang O. Efficient aerobic oxidation of ethylbenzene accelerated by cu species in hydrotalcite. Catalysis Communications. 2021 Jan 15; 149:106184.

[8] Chaudhary V, Sharma S. Synthesis of polymer-silica hybrid-supported catalysts for solvent-free oxidation of ethylbenzene with TBHP. Asia-Pacific Journal of Chemical Engineering. 2020 May;15(3): e2441.

[9] Chen Y, Jie S, Yang C, Liu Z. Active and efficient Co-N/C catalysts derived from cobalt porphyrin for selective oxidation of alkylaromatics. Applied Surface Science. 2017 Oct 15;419:98-106.

[10] Prawiranegara A, Sugesti H, Utama PS, Saputra E. Mn/Carbon Sphere Catalyst For Heterogeneous Activation Of Peroxymonosulfate For Methylene Blue Removal.

[11] Li H, Xu S, Du J, Tang J, Zhou Q. Cu@ Co-MOFs as a novel catalyst of peroxymonosulfate for the efficient removal of methylene blue. RSC advances. 2019;9(17):9410-20.

[12] Shokoohi R, Foroughi M, Latifi Z, Goljani H, Ansari A, Samarghandi MR, Nematollahi D. Comparing the performance of the peroxymonosulfate/Mn_3O_4 and three-dimensional electrochemical processes for

methylene blue removal from aqueous solutions: Kinetic studies. Colloid and Interface Science Communications. 2021 May 1;42:100394.

[13] Yu C, Wen M, Li S, Tong Z, Yin Y, Liu X, Li Y, Wu Z, Dionysiou DD. Elbaite catalyze peroxymonosulfate for advanced oxidation of organic pollutants: Hydroxyl groups induced generation of reactive oxygen species. Journal of Hazardous Materials. 2020 Nov 5;398:122932.

[14] Li Y, Liu Y, Liu Y, Chen Y, Chen L, Yan H, Chen Y, Xu F, Li M, Li L. Modification of sludge biochar by MnO_2 to degrade methylene blue: Synergistic catalysis and degradation mechanisms. Journal of Water Process Engineering. 2022 Aug 1;48:102864.

[15] Lei X, You M, Pan F, Liu M, Yang P, Xia D, Li Q, Wang Y, Fu J. $CuFe_2O_4$@ GO nanocomposite as an effective and recoverable catalyst of peroxymonosulfate activation for degradation of aqueous dye pollutants. Chinese Chemical Letters. 2019 Dec 1;30(12):2216-20.

[16] Li X, Lu H, Zhang Y, He F. Efficient removal of organic pollutants from aqueous media using newly synthesized polypyrrole/CNTs-$CoFe_2O_4$ magnetic nanocomposites. Chemical Engineering Journal. 2017 May 15;316:893-902.

[17] Dung NT, Thu TV, Van Nguyen T, Thuy BM, Hatsukano M, Higashimine K, Maenosono S, Zhong Z. Catalytic activation of peroxymonosulfate with manganese cobaltite nanoparticles for the degradation of organic dyes. RSC advances. 2020;10(7):3775-88.

[18] Kabel KI, Mady AH, Rabie AM. Novel preparation of ferromanganese oxide based on hyperbranched polymer for peroxymonosulfate activation as a robust catalyst for the degradation of organic pollutants. Environmental Technology & Innovation. 2021 May 1;22:101435.

[19] Zhang S, Fan Q, Gao H, Huang Y, Liu X, Li J, Xu X, Wang X. Formation of Fe_3O_4@ MnO_2 ball-in-ball hollow spheres as a high performance catalyst with enhanced catalytic performances. Journal of Materials Chemistry A. 2016;4(4):1414-22.

[20] Wang M, Wei Y, Zou Q, Zhang W, Xu A, Li X. Tuning manganese (III) species in manganese oxide octahedral molecular sieve by interaction with carbon nanofibers for enhanced pollutant degradation in the presence of peroxymonosulfate. Journal of colloid and interface science. 2019 Feb 15;536:271-80.

[21] Zhao X, Niu C, Zhang L, Guo H, Wen X, Liang C, Zeng G. Co-Mn layered double hydroxide as an effective heterogeneous catalyst for degradation of organic dyes by activation of peroxymonosulfate. Chemosphere. 2018 Aug 1;204:11-21.

[22] Gholami A, Mousavinia F. Eco-friendly approach for efficient catalytic degradation of organic dyes through peroxymonosulfate activated with pistachio shell-derived biochar and activated carbon. Environmental Technology. 2021 May 13:1-8.

[23] Li J, Zhang S, Chen Y, Liu T, Liu C, Zhang X, Yi M, Chu Z, Han X. A novel three-dimensional hierarchical CuAl layered double hydroxide with excellent catalytic activity for degradation of methyl orange. RSC advances. 2017;7(46):29051-7.

[24] Nguyen TD, Phan NH, Do MH, Ngo KT. Magnetic Fe_2MO_4 (M: Fe, Mn) activated carbons: fabrication, characterization and heterogeneous Fenton oxidation of methyl orange. Journal of Hazardous Materials. 2011 Jan 30;185(2-3):653-61.

[25] Qiu X, Yang S, Dzakpasu M, Li X, Ding D, Jin P, Chen R, Zhang Q, Wang XC. Attenuation of BPA degradation by SO4− in a system of peroxymonosulfate coupled with Mn/Fe MOF-templated catalysts and its synergism with Cl− and bicarbonate. Chemical Engineering Journal. 2019 Sep 15;372:605-15.

[26] Du J, Bao J, Liu Y, Kim SH, Dionysiou DD. Facile preparation of porous Mn/Fe3O4 cubes as peroxymonosulfate activating catalyst for effective bisphenol A degradation. Chemical Engineering Journal. 2019 Nov 15;376:119193.

[27] Li L, Zhang Q, She Y, Yu Y, Hong J. High-efficiency degradation of bisphenol A by heterogeneous Mn–Fe layered double oxides through peroxymonosulfate activation: Performance and synergetic mechanism. Separation and Purification Technology. 2021 Sep 1;270:118770.

[28] Zhang Z, Ding H, Li Y, Yu J, Ding L, Kong Y, Ma J. Nitrogen-doped biochar encapsulated Fe/Mn nanoparticles as cost-effective catalysts for heterogeneous activation of peroxymonosulfate towards the degradation of bisphenol-A: Mechanism insight and performance assessment. Separation and Purification Technology. 2022 Jan 15;283:120136.

[29] Li L, Huang Z, Liu Y, Zhu Z, Xu M, Wei W, Zhang Q, Hong J. Novel porous Mn-Fe nanocubes toward peroxymonosulfate activation via non-radical/radical pathways for emerging contaminants degradation. Applied Surface Science. 2022 Apr 15;581:152390.

[30] Xu S, Wen L, Yu C, Li S, Tang J. Activation of peroxymonosulfate by $MnFe_2O_4@$ BC composite for bisphenol A Degradation: The coexisting of free-radical and non-radical pathways. Chemical Engineering Journal. 2022 Aug 15;442:136250.

[31] Wang Q, Guan Z, Ding S, Xia D, Li D. Tuning the surface electronic state by the introduction of Mn on Fe2O3 to boost the activity of peroxymonosulfate. Separation and Purification Technology. 2022 May 15;289:120625.

[32] Kou L, Wang J, Zhao L, Jiang K, Xu X. Coupling of KMnO4-assisted sludge dewatering and pyrolysis to prepare Mn, Fe-codoped biochar catalysts for peroxymonosulfate-induced elimination of phenolic pollutants. Chemical Engineering Journal. 2021 May 1;411:128459.

[33] Hu F, Liu Y, Shi X, Xiao L. Removal of organic contaminants by starch-derived porous carbon via peroxymonosulfate activation: The role of N doping and Fe/Mn loading. Colloids and Surfaces A: Physicochemical and Engineering Aspects. 2022 Sep 20; 649:129520.

[34] Yao, Y., Cai, Y., Lu, F., Wei, F., Wang, X. and Wang, S., 2014. Magnetic recoverable $MnFe_2O_4$ and $MnFe_2O_4$-graphene hybrid as heterogeneous catalysts of peroxymonosulfate activation for efficient degradation of aqueous organic pollutants. *Journal of hazardous materials*, *270*, pp.61-70.

[35] Sharma, G., Kumar, A., Sharma, S., Ala'a, H., Naushad, M., Ghfar, A.A., Ahamad, T. and Stadler, F.J., 2019. Fabrication and characterization of novel $Fe^0@$ Guar gum-crosslinked-soya lecithin nanocomposite hydrogel for photocatalytic degradation of methyl violet dye. *Separation and Purification Technology*, *211*, pp.895-908.

[36] Othman I, Zain JH, Haija MA, Banat F. Catalytic activation of peroxymonosulfate using $CeVO_4$ for phenol degradation: an insight into the reaction pathway. Applied Catalysis B: Environmental. 2020 Jun 5;266:118601.

[37] Wan X, Qian D, Ai L, Jiang J. Highly efficient peroxymonosulfate activation by surface oxidized nickel phosphide with dual active sites. Industrial & Engineering Chemistry Research. 2020 Dec 8;59(51):22040-8.

[38] Yao Y, Hu Y, Hu H, Chen L, Yu M, Gao M, Wang S. Metal-free catalysts of graphitic carbon nitride–covalent organic frameworks for efficient pollutant destruction in water. Journal of colloid and interface science. 2019 Oct 15;554:376-87.

[39] Peng MM, Ganesh M, Vinodh R, Palanichamy M, Jang HT. Solvent free oxidation of ethylbenzene over Ce-BTC MOF. Arabian Journal of Chemistry. 2019 Nov 1;12(7):1358-64.

[40] Khare S, Singh Kirar J, Parashar S. Solvent-free oxidation of ethylbenzene over LDH-hosted Co (II) Schiff base of 2-hydroxy-1-naphthaldehyde and 4-amino benzoic acid. Inorganic and Nano-Metal Chemistry. 2019 Jul 3;49(7):204-16.

[41] Liu T, Cheng H, Sun L, Liang F, Zhang C, Ying Z, Lin W, Zhao F. Synthesis of acetophenone from aerobic catalytic oxidation of ethylbenzene over Ti–Zr–Co alloy catalyst: Influence of annealing conditions. Applied Catalysis A: General. 2016 Feb 25;512:9-14.

[42] Xie R, Fan G, Yang L, Li F. Hierarchical flower-like Co–Cu mixed metal oxide microspheres as highly efficient catalysts for selective oxidation of ethylbenzene. Chemical Engineering Journal. 2016 Mar 15;288:169-78.

[43] Qiu Y, Yang C, Huo J, Liu Z. Synthesis of Co-NC immobilized on carbon nanotubes for ethylbenzene oxidation. Journal of Molecular Catalysis A: Chemical. 2016 Dec 1;424:276-82.

[44] Dobras G, Sitko M, Petroselli M, Caruso M, Cametti M, Punta C, Orlińska B. Solvent-Free Aerobic Oxidation of Ethylbenzene Promoted by NHPI/Co (II) Catalytic System: The Key Role of Ionic Liquids. ChemCatChem. 2020 Jan 8;12(1):259-66.

[45] Zhou W, Dai X, Chen Y, Sun FA, He M, Chen Q. Synergistic catalytic oxidation of ethylbenzene to acetophenone by metallophthalocyanine intercalated layered double hydroxide with oxygen. ChemistrySelect. 2018 Jan 17;3(2):566-72.

[46] Huang G, Yuan RX, Peng Y, Chen XF, Zhao SK, Wei SJ, Guo WX, Chen X. Oxygen oxidation of ethylbenzene over manganese porphyrin is promoted by the axial nitrogen coordination in powdered chitosan. RSC advances. 2016;6(54):48571-9.

[47] Xiong Y, Sun W, Han Y, Xin P, Zheng X, Yan W, Dong J, Zhang J, Wang D, Li Y. Cobalt single atom site catalysts with ultrahigh metal loading for enhanced aerobic oxidation of ethylbenzene. Nano Research. 2021 Jul;14(7):2418-23.

[48] Zhou W, Lu W, Sun Z, Qian J, He M, Chen Q, Sun S. Fe assisted Co-containing hydrotalcites catalyst for the efficient aerobic oxidation of ethylbenzene to acetophenone. Applied Catalysis A: General. 2021 Aug 25;624:118322.

[49] Huang G, Mo LQ, Wei YX, Zhou H, Guo YA, Wei SJ. Effect of mesoporous chitosan action and coordination on the catalytic activity of mesoporous chitosan-grafted cobalt tetrakis (p-sulfophenyl) porphyrin for ethylbenzene oxidation. Catalysts. 2018 May;8(5):199.

[50] Huang G, Su TM, Zeng K, Guo YA, Zhao SK, Wei SJ. Mesoporous chitosan-immobilized iron tetrakis (4-carboxyphenyl) porphyrin as a model of cytochrome P-450 enzyme for oxidation of ethylbenzene. Applied Organometallic Chemistry. 2018 Mar;32(3):e4140.

[51] Habibi D, Faraji AR, Arshadi M, Veisi H, Gil A. Manganese nanocatalyst and N-hydroxyphthalimide as an efficient catalytic system for selective oxidation of ethylbenzene, cyclohexene and oximes under aerobic condition. Journal of Molecular Catalysis A: Chemical. 2014 Feb 1;382:41-54.

[52] Li X, Zhou L, Gao J, Miao H, Zhang H, Xu J. Synthesis of Mn3O4 nanoparticles and their catalytic applications in hydrocarbon oxidation. Powder Technology. 2009 Mar 25;190(3):324-6.

[53] Liu X, Gao S, Yang F, Zhou S, Kong Y. High promoting of selective oxidation of ethylbenzene by Mn-ZSM-5 synthesized without organic template and calcination. Research on Chemical Intermediates. 2020 May;46(5):2817-32.

[54] Liu M, Liu Y, Gao Z, Wang C, Ye W, Lu R, Zhang S. Nitrogen and sulfur co-doped carbon nanospheres for highly efficient oxidation of ethylbenzene. New Journal of Chemistry. 2018;42(19):15962-7.

[55] Yang L, Fan B, Cui X, Shi X, Li R. Solvent-free aerobic oxidation of ethylbenzene over Mn-containing silylated MgAl layered double hydroxides. Journal of Industrial and Engineering Chemistry. 2015 Jan 25;21:689-95.

[56] Faraji AR, Ashouri F, Hekmatian Z, Heydari S, Mosazadeh S. Organosuperbase dendron manganese complex grafted on magnetic nanoparticles; heterogeneous catalyst for green and selective oxidation of ethylbenzene, cyclohexene and oximes by molecular oxygen. Polyhedron. 2019 Jan 1;157:90-106.

[57] Al-Azmi A, Keshipour S. Cross-linked chitosan aerogel modified with Pd (II)/phthalocyanine: Synthesis, characterization, and catalytic application. Scientific reports. 2019 Sep 25;9(1):1-0.

[58] Xu WF, Chen WJ, Li DC, Cheng BH, Jiang H. Highly Dispersed Manganese Based $Mn/N–C/Al_2O_3$ Catalyst for Selective Oxidation of the C–H Bond of Ethylbenzene. Industrial & Engineering Chemistry Research. 2019 Feb 26;58(10):3969-77.

[59] L. Niu, G. Zhang, G. Xian, Z .Ren, T .Wei, Q. Li, Y. Zhang, Z. Zou. Tetracycline degradation by persulfate activated with magnetic $γ$-Fe_2O_3/CeO_2 catalyst: performance, activation mechanism and degradation pathway. Separation and Purification Technology. 259 (2021) 118156.

[60] Amasha M, Baalbaki A, Ghauch A. A comparative study of the common persulfate activation techniques for the complete degradation of an NSAID: the case of ketoprofen. Chemical Engineering Journal. 2018 Oct 15; 350:395-410.